International Journal Of Advancement In Engineering Technology, Management and Applied Science (IJAETMAS)
ISSN: 2349-3224 || www.ijaetmas.com || Volume 03 - Issue 11 || November - 2016 || PP. 27-41

Structure of non-viral vectors based on cholesteric liquid-crystal polymers by SAXS

M. Pérez Méndez[1], D. Rodríguez Martínez[2], J. Fayos[3]

[1]Institute of Polymer Science and Technology, CSIC, C/ Juan de la Cierva, 3. 28006 Madrid.
[2]Retinal degeneration: from genetics to therapy Laboratory, Centro Andaluz de Biología Molecular y Medicina Regenerativa Edif. CABIMER Avda. Américo Vespucio, s/n Parque Científico y Tecnológico Cartuja 93. 41092 Sevilla, Spain
[3]Instituto de Química-Física Rocasolano, CSIC, C/ Serrano 119. 28006 Madrid.

***Abstract* - Cationic polymers, at physiological pH, are used to condense anionic nucleic acids, as healing agent, into nano-sized particle-like complexes called "polyplexes", through self-assembly driven by electrostatic interactions. By compressing DNA molecules to a relatively small size, cellular internalization is facilitated and, thus, transfection efficacy is improved. New non-viral vector formulations are proposed for gene therapy.Cationic liquid-crystal polymers, synthetized as cholesteric and biocompatible, are directly complexed with polynucleotides of increasing complexity (both single and double stranded)or with two kinds of deoxyribonucleic acid (Plasmid PBR322 and calf-thymus DNA). Structural information of the polyplexes is studied by SAXS at the BM16 beamline at ESRF.The radii of gyration (R_g) of the Cholesteric Liquid-Crystal Polymer aggregates and polyplexes suspended in TAE, have been calculated from the slope of the corresponding Guinier plots *Ln (I) vs* q^2 (slope = $R_g^2/3$). Information about the shape is estimated by plotting *I(q) vs* $q*R_g$.Fractal nature is also analyzed from Porod plots*[Ln I(q)-B] vs Ln (q)*.The interaction between the new cationic cholesteric liquid-crystal polymers and oligonucleotides and DNA is confirmed in all the studied cases.**

Keywords: Cholesteric-liquid-crystal-polymers, cationic-polyplexes, SAXS, gene-therapy, non-viral vectors.

I. INTRODUCTION

In 1944, Erwin Schrödinger,in his book: *What is life? The physical aspect of the living cell* [1a], referring to the nature of the chromosome material, predicted the concept of ***"aperiodic crystal**, that in my opinion, is the material carrier of life…"* [1b]. Nine years before the structure of DNA fibers was determined by x-ray diffraction as a helical structure by Franklin [2a] and Wilkins [2b], and Watson and Crick reported the double helix, Fig.1, with periodic order along the sugar-phosphate helical backbone, every 34Å, and with ***aleatory*** distribution of the complementary bases pairs [2c]. The absence of lateral periodic order, coded by the peculiar sequence of base pairs along the structure, being convenient to endow DNA of their capacity to store genetic information.
In 1988 Ringsdorf established a parallel behavior between liquid-crystals in materials science and lipids in life science, due to their common amphiphilic nature, both being self-organizing systems [3].
Since 1992 the concept of crystal was re-defined by the International Union of Crystallography as: "Any solid which has a diffraction pattern essentially discrete" (Fourier space) [4], and the *Crystal Family* was accepted to be composed by: *Periodic* and *aperiodic crystals*. Liquid-crystals (LC) belong to the last group. The parallel orientation of their longitudinal molecular axes is common to all liquid-crystal mesophases (long-range orientational order), either nematic, smectic or cholesteric, Fig.2.
DNA behaves as liquid-crystal whith a cholesteric mesophase, shown in Fig.3, described as the special array of nematic planes, containing complementary base pairs, stacked in a super structure with chiral helical symmetry of charge distribution [5].

International Journal Of Advancement In Engineering Technology, Management and Applied Science (IJAETMAS)
ISSN: 2349-3224 || www.ijaetmas.com || Volume 03 - Issue 11 || November - 2016 || PP. 27-41

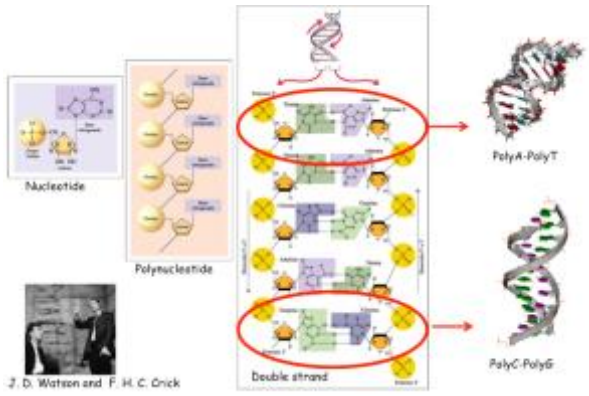

Fig. 1. DNA crystal structure according to [2c]. Detail of double stranded PolyA-PolyT and PolyC-PolyG are shown at the right hand side.

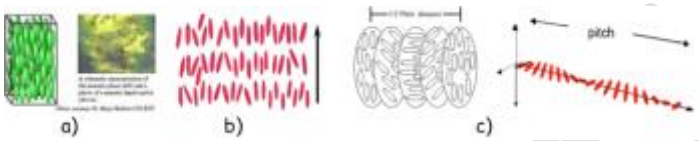

Fig. 2. Types of Liquid-Crystal mesophases: a) Nematic, b) Smectic A and c) Cholesteric, helical pitch.

Fig. 3. Cholesteric mesophase of liquid-crystal DNA

1.1. Synthetic cholesteric liquid-crystal polymers

Two multifunctional cholesteric liquid-crystal polymers (ChLCP), named PTOBEE and PTOBDME, with chemical formulations in Fig.4, were synthetized in our laboratory -through a polycondensation reaction [6]- as optically active materials, being characterized by NMR, Raman spectroscopy, steady-state fluorescence, molecular modeling, and SAXS/WAXS [7], [8].

These ChLCP behave as thermotropic and lyotropic, confering interesting macromolecular properties indicative of potential application on the biomedical and engineering field. They have shown to be biocompatible against macrophages and fibroblasts cellular lines. Besides they are able to interact with biomacromolecules such as lipids (both neutral and cationic) and with polynucleotides and nucleic acids.

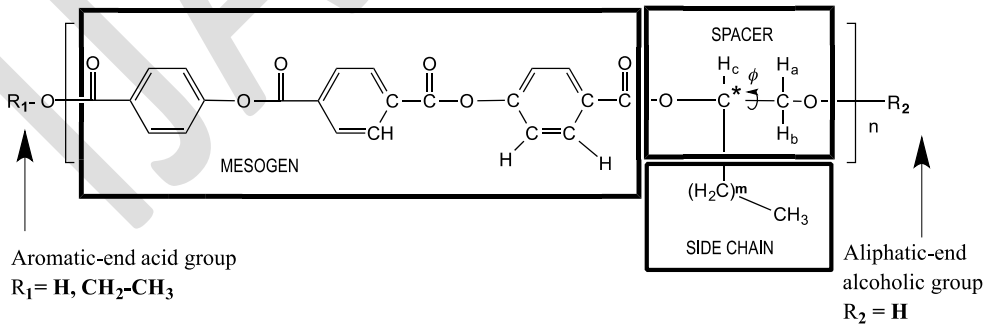

Fig. 4. Monomeric unit of cholesteric liquid-crystalline PTOBEE (m=1) and PTOBDME (m=9). The three different zones of the monomer: mesogen, spacer and flexible side chain are indicated. The asterisk indicates the chiral center. Torsion ϕ is indicated. Aromatic-end acid and aliphatic-end alcoholic groups are also specified.

1.2. Interaction with lipids.

These cholesteric liquid-crystal polyesters have shown to be able to interact with lipids. Fig.5 shows hexagonal liposomes of L-α–DMPC when interacting with PTOBDME. The structures of the lipid membranes complexed with ChLCP were analyzed by simultaneous SAXS/WAXS with synchrotron radiation monochromatic beam λ=1.5 Å on the X33 camera at EMBL (DESY, Hamburg) [9, 10, 11]. Both linear detectors were calibrated using Tripalmitin. Data were normalized for incident intensity and analyzed by using the program Primus (ATSAS) [12].

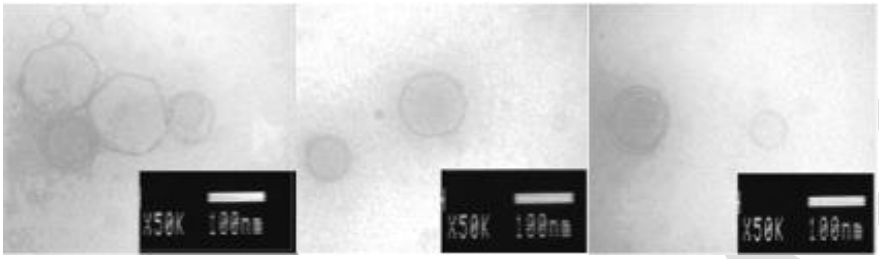

Fig. 5. TEM images of L-α-DMPC liposomes, hexagonal when interacting with added PTOBDME.

1.3. Interaction with polynucleotides and nucleic acids. Non-viral vectors.

The introduction of exogenous genetic material in cells is a key stage in the development of basic research in cellular biology. The term "transfection" is used to indicate the transfer of DNA- as healing agent- into the nuclei of cells of higher organisms. The direct application of this technology in living organisms opens many possibilities, as gene therapy and vaccines using DNA [13].

The development of new non-viral vectors requires synthetic molecules that can bind polynucleotide fragments (the therapeutic agent) and transfect cells, but not stimulate an immune response.

Cationic polymers, at physiological pH, are used to condense anionic nucleic acids into nano-sized particle-like complexes called "polyplexes", through self-assembly driven by electrostatic interactions. By compressing DNA molecules to a relatively small size cellular internalization is facilitated and, thus, transfection efficacy is improved [14].

The cholesteric LC nature of our polymers, similar to that of DNA, makes them good candidates for new cationic formulations. Polyplexes including PTOBEE and/or PTOBDME and new synthetized monomeric cationic surfactant molecules, were developed in our lab to entrap an anionic plasmid of DNA. These polyplexes were successfully tested as non-viral vectors in gene therapy, both *in vitro* and *in vivo.* Their structures were identified by synchrotron radiation source [11, 15, 16].

Cationic functionalized ChLCP, PTOBEE-NH_2, was synthesized and directly complexed with anionic commercial polynucleotide PolyC-PolyG. Neutron scattering experiments, had shown sufficient contrast (scattering length density difference) between PTOBEE-NH_2 ($1.887x10^{10}/cm^2$) and [PolyC-PolyG] ($3.32x10^{10}/cm^2$) for contrast variation SANS experiments. This experiment was successfully performed at NIST [17].

In this work, new cationic ChLCP have been synthetized and directly complexed with polynucleotides both single and double stranded and with two kinds of deoxyribonucleic acid (Plasmid PBR322 and calf thymus). Structural information of the complexes is studied by SAXS at the BM16 beamline at ESRF.

II. METHODS

2.1. Materials and samples preparation.

Cationic cholesteric liquid-crystal polymers were synthetized by functionalizing PTOBDME, and PTOBEE with ammonium and choline groups and were characterized by NMR and DSC [18].

Polynucleotides and nucleic acids were acquired from Sigma-Aldrich (Spain). Table1 summarizes their structural aspects.

The cationic complexes were obtained by suspending the cholesteric LC polymers in (Tris Acetate: EDTA) buffer (0.04M TRIS: 0.001M EDTA) at room temperature, and directly mixing, with different single stranded polynucleotide: [Poly-A]; [Poly-C]; [Poly-G]; [PolydT]; or double stranded [PolyC-PolyG]; [PolyA-PolydT], and with different nucleic acids: calf thymus DNA or plasmid PBR322. Three different

proportions ChLCP:DNA were studied in all cases: (1:2), (1:1), and (2:1) respectively, being all of them mixed and digested for 12h in a swinging shaker.

Table 1.
Molecular weights and structure of commercial polynucleotides and nucleic acids.

Sample	Molecular Weight	Structure
PolyA	200.000 to 700.000	Single strand
PolyC	Not determined	Single strand
PolyG	80.000 to 500.000	Single strand
PolydT	Not determined	Single strand
PolyA-PolydT_{10}	Not determined	Double strand
PolyG-PolyC	300.000	Double strand
Deoxyribonucleic Acid (Plasmid PBR322)	2.900.000	Double strand
Deoxyribonucleic Acid (Calf Thymus)	10.000.000 to 15.000.000	Double strand

2.2. Characterization Technique.

SAXS experiment was performed at the BM16 beamline at ESRF. A monochromatized beam at λ= 0,98 Å was used. An image-plate detector was placed at 6 m from the sample to collect two-dimensional data. The program Fit2D was employed to evaluate the beam center position and to generate a mask file. Binary data are normalized by the detector response and pixels are radially averaged into 1D. Silver behenate (d= 58.3 Å) was used to calibrate the angular axis.

The radii of gyration (R_g) have been calculated from the slope of the corresponding Guinier plots *Ln (I) vs* q^2 (slope = $R_g^2/3$). The Guinier region corresponds to the range $QR_g < \sqrt{3}$.

The Porod plot *[Ln I(q)-B] vs Ln (q)]* for scattering objects with smooth interfaces, yields an exponent from the slope. A slope $n = 1$ is obtained for scattering from rigid rods; a slope $n = 4$ represents a scattering particle with smooth surface; whereas a slope n between 3 and 4 characterizes rough interfaces of fractal dimension D with n = 6-D. This is called a surface fractal [19].

In the case of polymer coils, the Porod slope $n = 2$ is a signature of Gaussian chains in a dilute environment, a slope $n = 5/3$ is for *fully swollen coils* and a slope $n = 3$ is for *collapsed polymer coils*. A slope between 2 and 3 is for *"mass fractals"* such as branched systems (gels) or networks.

Information about the shape of the ChLCP aggregates, suspended in TAE, is estimated by plotting *I(q) vs* $q*R_g$. Structural analysis of some cationic complexes is proposed with the combination of program ATSAS [12].

II. RESULTS AND DISCUSSION.

The R_g values (nm) of synthetic cationic cholesteric liquid crystal polymers: PTOBEE-Choline, PTOBDME-Choline, PTOBEE-Ammonium and their precursors PTOBEE and PTOBDME, dispersed in TAE at 10, 7, 5, 2.5 and 1(mg/ml), respectively, are given in Table 2.

Table 2
R_g values (nm) of cationic ChLCP and precursors, in TAE, calculated from the Guinier plots.

	10 mg/ml	7 mg/ml	5 mg/ml	2,5 mg/ml	1 mg/ml
PTOBEE	32,8	32,62	32,57	32,96	34,28
PTOBDME	40,88	40,11	39,72	38,22	38,36
PTOBEE- Choline	39,06	39	39,13	39,13	39,6
PTOBEE-Ammonium	40,40	40,0	40,13	40,00	40,02
PTOBDME- Choline	42,30	41,42	41,7	41,38	41,27

Precursor PTOBDME (with ten carbon atoms in lateral hydrophobic chains) exhibits higher R_g values than PTOBEE (with only two carbon atoms in lateral chains) in all the studied concentrations, for the solvent under study. The discrete difference in their size is interpreted as due to the self-organization of both polymers in nano aggregates, hindering their lateral chains by the effect of polar solvent. The functionalization with choline groups increases the size of the polymers with respect to their precursor in

International Journal Of Advancement In Engineering Technology, Management and Applied Science (IJAETMAS)
ISSN: 2349-3224 || www.ijaetmas.com || Volume 03 - Issue 11 || November - 2016 || PP. 27-41

both cases, with PTOBDME-Choline having the higher R_g values of those studied. PTOBEE-Ammonium shows even higher size aggregates than PTOBEE-Choline.
Fig.6 shows the *I(q) vs* $q*R_g$ plots for the synthetic liquid crystal polymers in TAE. As the polymer concentration increases an evolution from rods, in the case of PTOBEE and PTOBDME-Choline (1mg/ml) to disks and spheres (10mg/ml in all cases) is observed. PTOBEE-Ammonium seems to form spheres in all the studied concentrations.

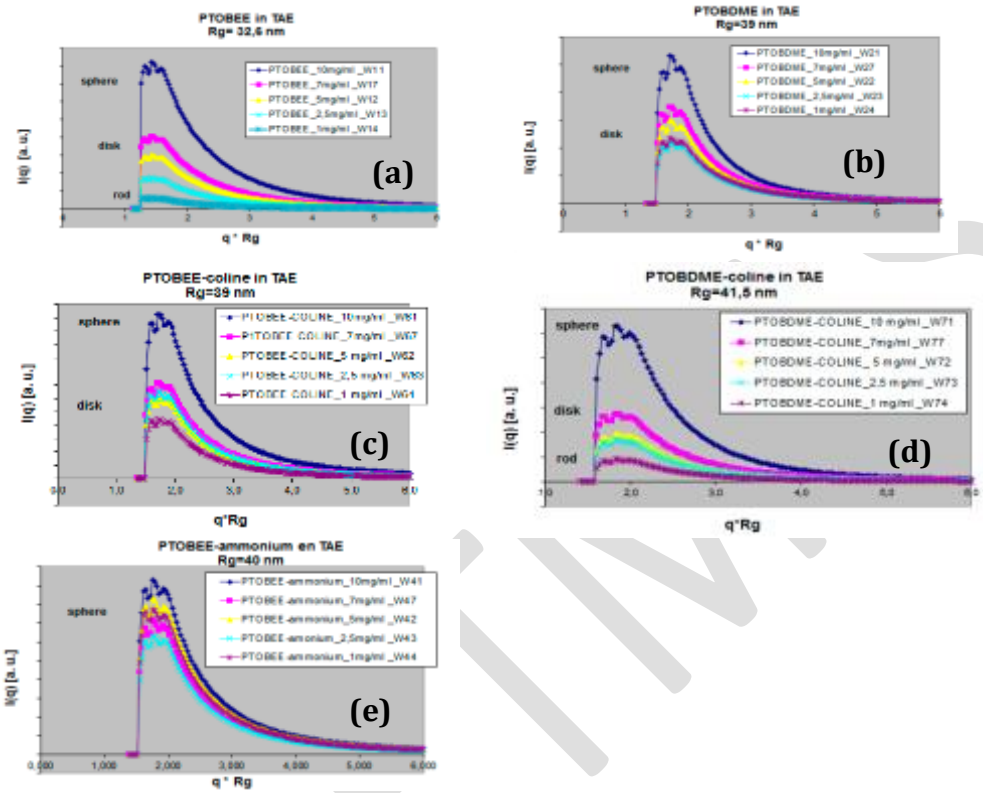

Fig. 6.*I(q) vs* $q*R_g$curves for: (a) PTOBEE; (b) PTOBDME; (c) PTOBEE-Choline; (d) PTOBDME-Choline and(e)PTOBEE-Ammoniun.

In Fig.7 the *I(q) vs q* (nm^{-1}) are ploted from experimental SAXS data of the commercial polynucleotides and nucleic acids. A big difference in intensity is observed for plasmid DNA, with respect to the rest. This suggests the presence of calf-thymus DNA, with the highest molecular weight in Table 1, in a supercoiled state.

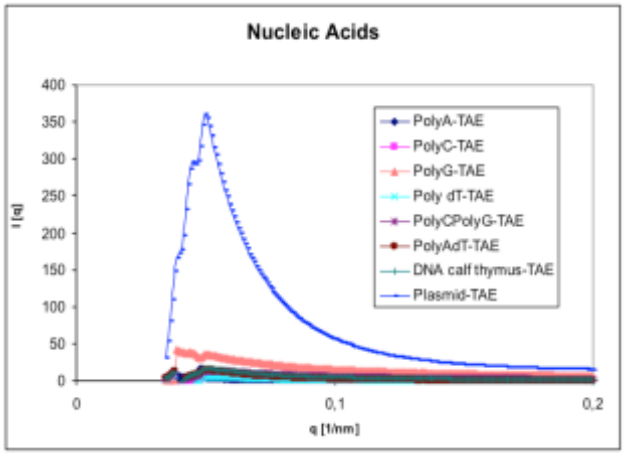

Fig. 7.*I(q) vsq*(nm^{-1}) plots of: PolyA, PolyC, PolyG, PolydT, PolyC-PolyG, PolyA-PolydT, Calf Thymus DNA and Plasmid, in TAE

Fig.8 enhibits the SAXS curves *I(q) vs q [nm^{-1}]* of PolyA and their polyplexes with PTOBDME-Choline, PTOBEE-Choline and PTOBEE-Ammonium, compared to the isolated polymer PTOBDME-Choline (at 10 mg/ml). Their calculated R_g values, shape and fractal nature are described in Table 3.

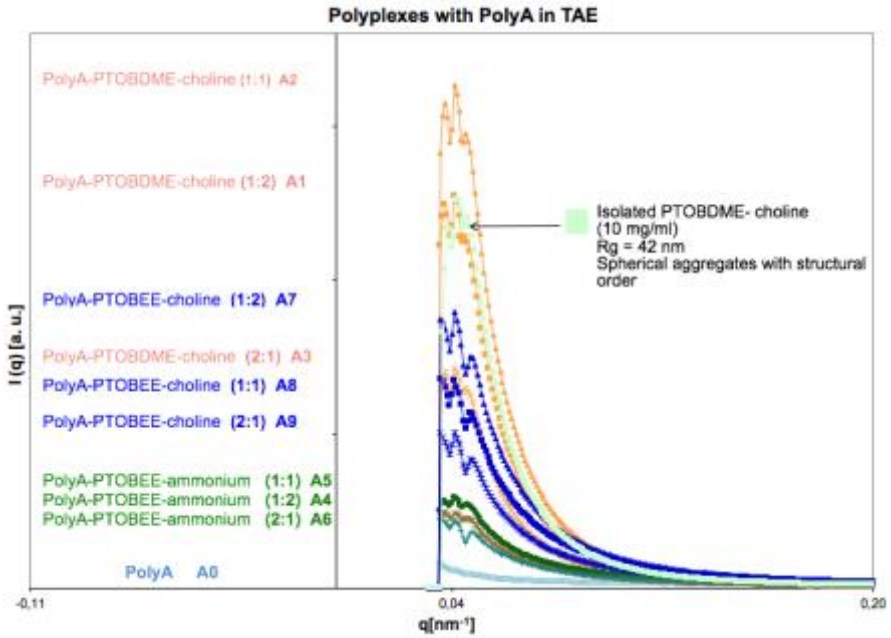

Fig. 8. SAXS curves *I(q) vs q[nm^{-1}]* for PolyA and polyplexes with PTOBDME-Choline, PTOBEE-Choline and PTOBEE-Ammonium, in TAE.

Table 3
Calculated R_g Guinier (nm) from SAXS curves, shape and fractal nature of Polyplexes with PolyA

	Guinier Region Rg [nm]	Shape I(q) versus q*R	Porod Slope Ln [I(q)-B] *vs* Ln (q)
PolyA A0	33,94	Rod	-1,6 *fully swollen coils*
PolyA-PTOBDME-choline (1:2) A1	40,37	shpere	-3,6 *rough interface of fractal dimension*
PolyA-PTOBDME-choline (1:1) A2	41,02	sphere	-3,7 *rough interface of fractal dimension*
PolyA-PTOBDME-choline (2:1) A3	39,8	sphere	-3,5 *rough interface of fractal dimension*
PolyA-PTOBEE_ammonium (1:2) A4	37,4	"	-2,4 *complex mass fractal (network)*
PolyA-PTOBEE_ammonium (1:1) A5	37,4	"	-2,5 *complex mass fractal (network)*
PolyA-PTOBEE_ammonium (2:1) A6	35,53	"	-2,26 *complex mass fractal (network)*
PolyA-PTOBEE-choline (1:2) A7	37,33	"	-2,78 *complex mass fractal (network)*
PolyA-PTOBEE-choline (1:1) A8	36,32	"	-2,63 *complex mass fractal (network)*
PolyA-PTOBEE-choline (2:1) A9	36,38	"	-2,56 *complex mass fractal (network)*

Isolated PolyA, seems to be present as rod-like aggregates with a Porod slope tipical of *fully swollen coils*. In the complexes the R_g have values intermediate between PolyA and their respective cationic ChLCPs, probably due to strong electrostatic interaction, with formation of complex *mass fractal networks* in the case of PTOBEE-Ammonium and PTOBEE-Choline and *rough interface of fractal dimension* in the case of PTOBDME-Choline.

The SAXS curves of polyplexes formed with PolydT are given in Fig. 9. Table 4 shows the calculated R_g for Poly dT and their complexes. A Porod slope near to that of *fully swollen coil* is foundfor PolydT and *rough interface of fractal dimension* for (PolydT-PTOBEE-Ammonium) in proportions (1:2) and (1:1). The rest of complexes seems to be as *complex mass fractal (network)*, with disk shape

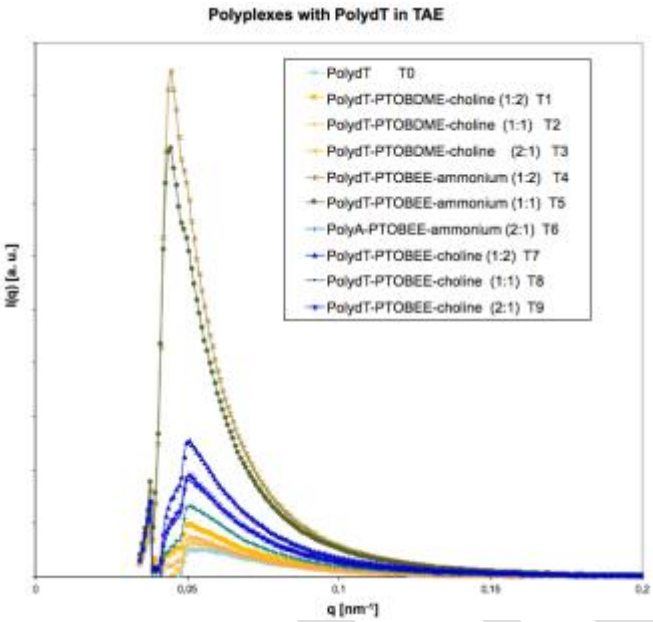

Fig. 9. SAXS curves *I(q) vs q[nm^{-1}]* for PolydT and polyplexes with PTOBDME-Choline, PTOBEE-Choline and PTOBEE-Ammonium, in TAE.

Table 4
Calculated R_g Guinier (nm) from SAXS curves, shape and fractal nature of Polyplexes with PolydT

		Guinier Region Rg [nm]	Shape I(q) versus q*R	Porod Slope Ln [I(q)-B] *vs* Ln (q)
PolydT	T0	27,044	Rod	-1,86 *fully swollen coils*
PolydT-PTOBDME-choline (1:2)	T1	29,89	Disc	-2,48 *mass fractals (network)*
PolydT-PTOBDME-choline (1:1)	T2	26,8	Disc	-2,06 *mass fractals (network)*
PolydT-PTOBDME-choline (2:1)	T3	29,23	Disc	-2,42 *mass fractals (network)*
PolydT-PTOBEE_ammonium (1:2)	T4	40,75	Sphere	-3,45 *rough interface of fractal dimension*
PolydT-PTOBEE_ammonium (1:1)	T5	39,68	"	-3,35 *rough interface of fractal dimension*
PolydT-PTOBEE_ammonium (2:1)	T6	29,13	Disc	-2,53 *mass fractals (network)*
PolydT-PTOBEE-choline (1:2)	T7	33,14	"	-2,72 *mass fractals (network)*
PolydT-PTOBEE-choline (1:1)	T8	30,86	"	-2,58 *mass fractal (network)*
PolydT-PTOBEE-choline (2:1)	T9	31,77	"	-2,37 *mass fractal (network)*

SAXS curves of polyplexes of cationic ChLCP complexed with PolyC are shown in Fig. 10; and with PolyG in Fig. 11. Their respective calculated Guinier R_g values in (nm), shape and fractal nature of Polyplexes with PolyC are in Table 5, and with PolyG in Table 6. Isolated PolyC presents a Porod slope tipical of *Gaussian chains in a dilute environment*, slightly towards a *mass fractal*. It seems to aggregate in a more globular form than the other single stranded polynucleotides. The complexes (PolyC-PTOBDME-choline) are the most voluminous with *rough interface of fractal dimension*. The rest of the polyplexes with PolyC have present *mass fractal (network)* texture. According to Table 6, PolyG behaves as *scattering rigid rods*. Complexes (PolyG-PTOBDME-choline) present *rough interface of fractal dimension* in the three studied proportions. Complex (PolyG-PTOBEE-ammonium) (2:1) has a slope value as *fully swollen coils*, while complex (PolyG-PTOBEE-ammonium) (1:1) approaches a *gaussian chains* structure and (PolyG-

PTOBEE-ammonium) (1:2) aggregates as *mass fractal (network).* Polyplexes (PolyG-PTOBEE-choline) show *mass fractal (network)* in the three studied proportions.

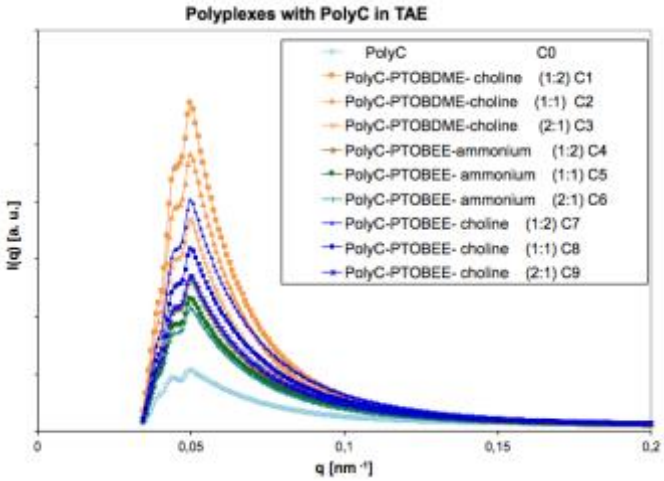

Fig. 10. SAXS curves *I(q) vs q[nm^{-1}]* for PolyC and polyplexes with PTOBDME-Choline, PTOBEE-Choline and PTOBEE-Ammonium, in TAE.

Table 5
Calculated R_g Guinier (nm) from SAXS curves, shape and fractal nature of Polyplexes with PolyC.

		Guinier Region Rg [nm]	Shape I(q) versus q*R	Porod Slope Ln [I(q)-B] *vs* Ln (q)
PolyC	C0	24,5	Rod	-2,16 *Gaussian chains*
PolyC-PTOBDME-choline (1:2)	C1	38,02	Sphere	-3,6 *rough interface of fractal dimension*
PolyC-PTOBDME-choline (1:1)	C2	37,78	sphere	-3,6 *rough interface of fractal dimension*
PolyC-PTOBDME-choline (2:1)	C3	36,77	sphere	-3,4 *rough interface of fractal dimension*
PolyC-PTOBEE_ammonium (1:2)	C4	34,015	Disc	-2,86 *mass fractal (network)*
PolyC-PTOBEE_ammonium (1:1)	C5	33,20	"	-2,5 *mass fractal (network)*
PolyC-PTOBEE_ammonium (2:1)	C6	32,36	Disc	-2,41 *mass fractal (network)*
PolyC-PTOBEE-choline (1:2)	C7	34,58	"	-2,61 *mass fractal (network)*
PolyC-PTOBEE-choline (1:1)	C8	33,94	"	-2,54 *mass fractal (network)*
PolyC-PTOBEE-choline (2:1)	C9	33,14	"	-2,48 *mass fractal (network)*

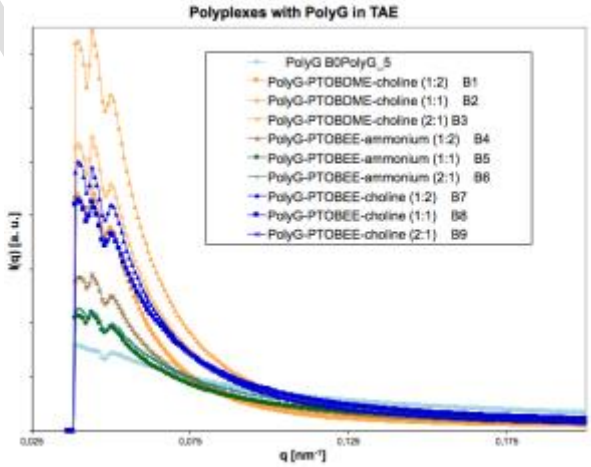

Fig. 11. SAXS curves I(q) *vs q[nm^{-1}]* for PolyG and polyplexes with PTOBDME-Choline PTOBEE-Choline and PTOBEE-Ammonium, in TAE.

Table 6
Calculated R_g Guinier (nm) from SAXS curves, shape and fractal nature of Polyplexes with PolyG

		Guinier Region Rg [nm]	Shape I(q) versus q*R	Porod Slope Ln [I(q)-B] *vs* Ln (q)
PolyG	B0	21,043	Rod	-1,03 *scattering rigid rods*
PolyG-PTOBDME-choline (1:2)	B1	38,86	Sphere	-3,34 *rough interface of fractal dimension*
PolyG-PTOBDME-choline (1:1)	B2	37,95	sphere	-3,1 *rough interface of fractal dimension*
PolyG-PTOBDME-choline (2:1)	B3	36,05	sphere	-3,5 *rough interface of fractal dimension*
PolyG-PTOBEE_ammonium (1:2)	B4	34,86	Disc	-2,4 *mass fractal (network)*
PolyG-PTOBEE_ammonium (1:1)	B5	32,21	"	-1,9 *gaussian chains*
PolyG-PTOBEE_ammonium (2:1)	B6	30,276	Disc	-1,67 *fully swollen coils*
PolyG-PTOBEE-choline (1:2)	B7	36,77	Sphere	-2,62 *mass fractal (network)*
PolyG-PTOBEE-choline (1:1)	B8	34,68	"	-2,27 *mass fractal (network)*
PolyG-PTOBEE-choline (2:1)	B9	34,68	"	-2,27 *mass fractal (network)*

The SAXS patterns of cationic ChLCPs complexed with (PolyC-PolyG) and with (PolyA-PolyT) are given in Fig.12 and Fig. 13 respectively.

The estimated R_g Guinier (nm), shape and fractal nature of Polyplexes with PolyC-PolyG are given in Table 7, and those of (PolyA-PolyT) in Table 8.

Polynucleotide (PolyC-PolyG) dispersed in TAE, shows gradient corresponding to fully *swollen coils* (1,6). Fitting of PolyC-PolyG SAXS pattern to a rod model with GNOM (ATSAS) [12] is shown in Fig. 12b. Complexes (PolyC-PolyG-PTOBDME-choline), in the three studied proportions, present globular monodispersed aggregates with a Porod slope interpreted as due to *collapsed coils*. All proportions of complexes (PolyC-PolyG-PTOBEE-ammonium) and (PolyC-PolyG-PTOBEE-choline) exhibit globular monodispersed gradients corresponding to *mass fractals network.*

PolyA-PolyT, with the higher Porod gradient (2,8) among the polynucleotides studied, seems to be present as *globular monodispersed –collapsed coils*. The whole of their complexes show can be modelized by globular monodispersed aggregates with *collapsed coils* gradient.

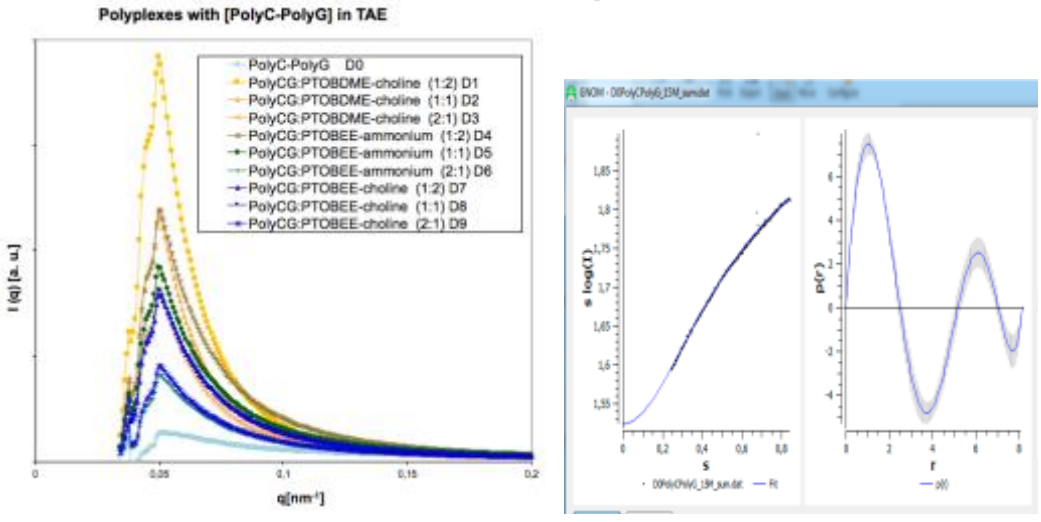

(a) **(b)**

Fig. 12.(a) SAXS patterns of Complexes between PolyC-PolyG and cationic ChLCPs; (b) Fitting PolyC-PolyG to a rod model with ATSAS [12]

Table 7
Calculated R_g Guinier (nm) from SAXS curves, shape and fractal nature of Polyplexes with PolyC-PolyG

	Guinier R. Rg [nm]	Shape I(q) versus q*R	Porod Slope Ln [I(q)-B] *vs* Ln (q)
PolyC-PolyG D0	18,8	Rod	-1,6 *fully swollen coils*
PolyC-PolyG -PTOBDME-choline (1:2) D1	39,12	Globular monidisp	-3,6 *collapsed coils*
PolyC-PolyG -PTOBDME-choline (1:1) D2	38,09	Globular monidisp	-3,37 *collapsed coils*
PolyC-PolyG -PTOBDME-choline (2:1) D3	36,75	Globular monidisp	-3,10 *collapsed coils*
PolyC-PolyG -PTOBEE_ammonium (1:2) D4	33,89	Globular monidisp	-2,64 *mass fractal*
PolyC-PolyG -PTOBEE_ammonium (1:1) D5	34,24	Globular monodisp	-2,64 *mass fractals*
PolyC-PolyG -PTOBEE_ammonium (2:1) D6	31,02	Globular monidisp	-2,31 *mass fractals*
PolyC-PolyG -PTOBEE-choline (1:2) D7	33,69	Globular monodisp	-2,64 *mass fractals*
PolyC-PolyG -PTOBEE-choline (1:1) D8	33,85	Globular monodisp	-2,66 *mass fractals*
PolyC-PolyG -PTOBEE-choline (2:1) D9	31,77	Globular monodisp	-2,37 *mass fractals*

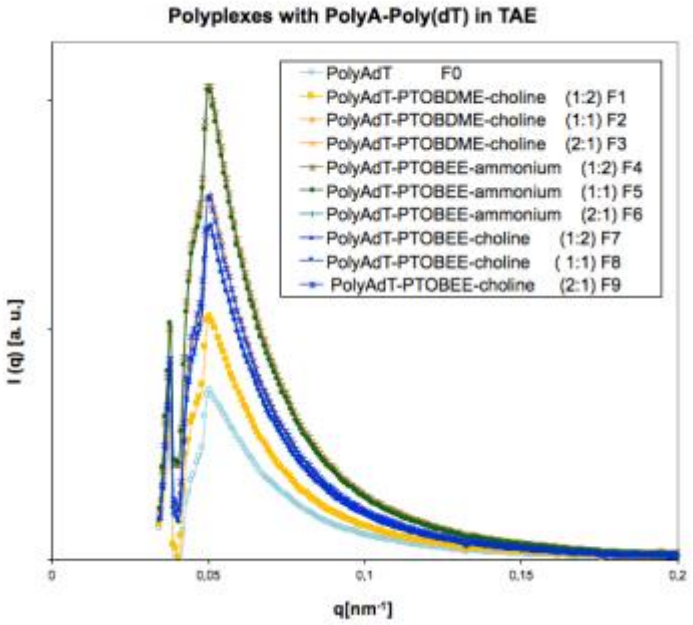

Fig. 13. SAXS patterns of Complexes between PolyA-PolyT and cationic ChLCPs.

Table 8
Calculated R_g Guinier (nm) from SAXS curves, shape and fractal nature of Polyplexes with PolyA-PolyT

	Guinier Region Rg [nm]	Shape I(q) versus q*R	Porod Slope Ln [I(q)-B] *vs* Ln (q)
PolyAdT F0	31,8	Globular	-2,87 *Collapsed coils*
PolyAdT -PTOBDME-choline (1:2) F1	33,36	Globular monidisp	-3,0 *Collapsed coils*
PolyAdT -PTOBDME-choline (1:1) F2	34,75	Globular monidisp	-2,98 *Collapsed coils*
PolyAdT -PTOBDME-choline (2:1) F3	35,13	Globular monidisp	-2,95 *Collapsed coils*
PolyAdT -PTOBEE_ammonium (1:2) F4	34,95	Globular monidisp	-2,96 *Collapsed coils*
PolyAdT -PTOBEE_ammonium (1:1) F5	35,17	Globular monodisp	-3,03 *Collapsed coils*
PolyAdT -PTOBEE_ammonium (2:1) F6	34,73	Globular monidisp	-3,0 *Collapsed coils*
PolyAdT -PTOBEE-choline (1:2) F7	34,41	Globular monodisp	-3,0 *Collapsed coils*
PolyAdT -PTOBEE-choline (1:1) F8	34,40	Globular monodisp	-2,99 *Collapsed coils*
PolyAdT -PTOBEE-choline (2:1) F9	34,47	Globular monodisp	-3,01 *Collapsed coils*

SAXS curves of cationic ChLCPs complexes with calf–thymus DNA and plasmid DNA are in Fig.14 and Fig. 15, respectively. Shape estimation, modelized to a globular monodispersed system model with the help of GNOM (ATSAS) is reported for all the studied complexes in Table 9 and Table 10. In Fig. 15b the fitting model of the plasmid is shown.

The Porod gradient of isolated calf-thymus, suspended in TAE (-1,6 full) corresponds to *swollen coils*. While complexes (Calf-Thymus DNA-PTOBDME-choline) aggregate as *collapsed coils*, in all proportions, (Calf-Thymus DNA-PTOBEE-ammonium) and (Calf-Thymus DNA-PTOBEE-choline) self-associate as *mass fractal network.*

The gradient= -3,2 of the plasmid DNA, in Fig. 15, is interpreted as due to *collapsed coils* with globular particles shape. Polyplexes (Plasmid_DNA-PTOBDME-choline) and (Plasmid_DNA-PTOBEE-Ammonium (1:2) have gradients for *collapsed coils*. The rest of the complexes with Plasmid DNA have *mass fractal* Porod slopes.

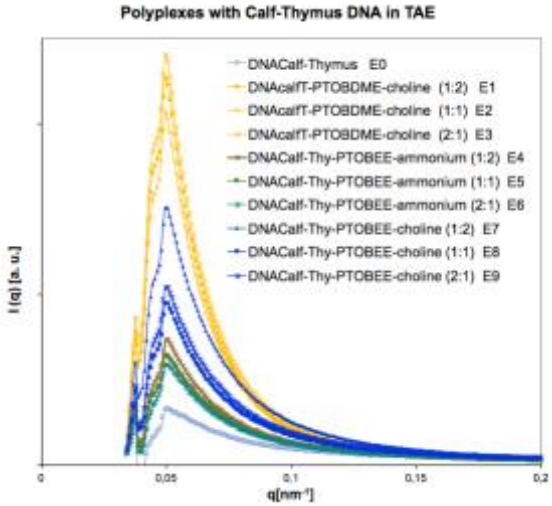

Fig. 14. SAXS patterns of Complexes between Calf-Thymus DNA and cationic ChLCPs.

Table 9
Calculated R_g Guinier (nm) from SAXS curves, shape and fractal nature of Polyplexes with Calf-Thymus DNA

	Guinier R. Rg [nm]	Shape I(q) versus q*R	Porod Slope Ln [I(q)-B] *vs* Ln (q)
Calf-thymus DNA E0	26,6	Globular monidisp	-1,55 *Fully swollen coils*
Calf-thymus DNA-PTOBDME-choline (1:2) E1	38,90	Globular monidisp	-3,21 *Collapsed coils*
Calf-thymus DNA-PTOBDME-choline (1:1) E2	38,26	Globular monidisp	-3,11 *Collapsed coils*
Calf-thymus DNA-PTOBDME-choline (2:1) E3	38,63	Globular monidisp	-3,17 *Collapsed coils*
Calf-thymus DNA-PTOBEE_ammonium (1:2) E4	32,96	Globular monidisp	-2,32 *Mass fractal*
Calf-thymus DNA-PTOBEE_ammonium (1:1) E5	32,16	Globular monodisp	-2,44 *Mass fractals*
Calf-thymus DNA-PTOBEE_ammonium (2:1) E6	31,43	Globular monidisp	-2,36 *Mass fractals*
Calf-thymus DNA-PTOBEE-choline (1:2) E7	34,12	Globular monodisp	-2,63 *Mass fractals*
Calf-thymus DNA-PTOBEE-choline (1:1) E8	33,23	Globular monodisp	-2,54 *Mass fractals*
Calf-thymus DNA-PTOBEE-choline (2:1) E9	33,25	Globular monodisp	-2,53 *Mass fractals*

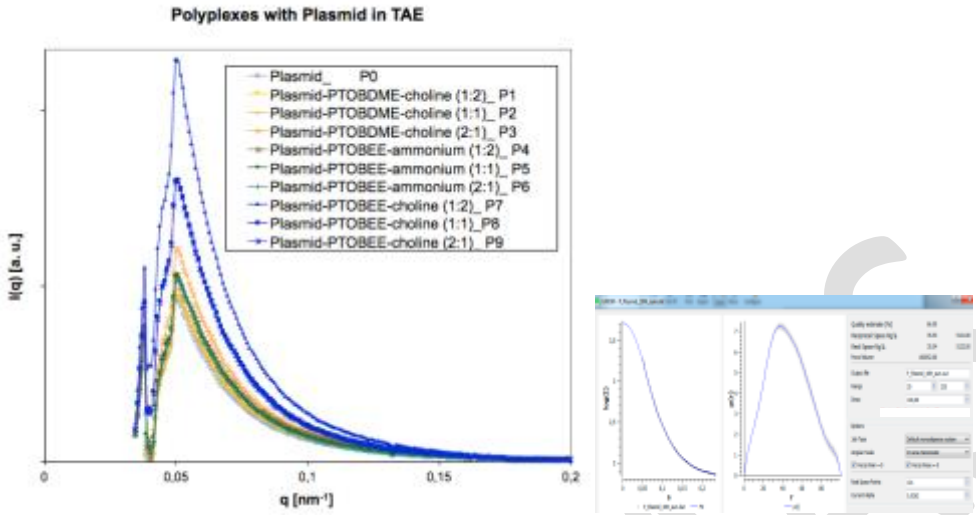

(a) **(b)**

Fig. 15. (a) SAXS patterns of Complexes between Plasmid DNA and cationic ChLCPs; (b) Fitting the plasmid to a globular monodispersed system model with GNOM (ATSAS) [12].

Table 10
Calculated R_g Guinier (nm) from SAXS curves, shape and fractal nature of Polyplexes with Plasmid_DNA

	Guinier Region Rg [nm]	Shape I(q) versus q*R	Porod Slope Ln [I(q)-B] *vs* Ln (q)
Plasmid_DNA P0	34,22	Globular monidisp	-3,2 *Collapsed coils*
Plasmid_DNA-PTOBDME-choline (1:2) P1	33,38	Globular monidisp	-3,12 *Collapsed coils*
Plasmid_DNA-PTOBDME-choline (1:1) P2	33,17	Globular monidisp	-3,0 *Collapsed coils*
Plasmid_DNA-PTOBDME-choline (2:1) P3	33,66	Globular monidisp	-3,0 *Collapsed coils*
Plasmid_DNA-PTOBEE_ammonium (1:2) P4	32,99	Globular monidisp	-3,06 *Collapsed coils*
Plasmid_DNA-PTOBEE_ammonium (1:1) P5	33,66	Globular monodisp	-2,73 *Mass fractals*
Plasmid_DNA-PTOBEE_ammonium (2:1) P6	33,79	Globular monidisp	-2,74 *Mass fractals*
Plasmid_DNA-PTOBEE-choline (1:2) P7	35,22	Globular monodisp	-2,94 *Mass fractals*
Plasmid_DNA-PTOBEE-choline (1:1) P8	34,35	Globular monodisp	-2,82 *Mass fractals*
Plasmid_DNA-PTOBEE-choline (2:1) P9	34,37	Globular monodisp	-2,83 *Mass fractals*

IV. CONCLUSIONS

The present investigation reveals that cationic cholesteric liquid-crystal polymers: PTOBEE-choline, PTOBDME-choline, PTOBEE-ammonium and precursors PTOBEE and PTOBDME, dispersed in TAE at 10mg/ml, 7mg/ml, 5mg/ml, 2,5mg/ml and 1mg/ml, respectively, self-assembly in nano aggregates with R_g values estimated from the SAXS data.
Precursor PTOBDME, with ten carbon atoms in their lateral hydrophobic chains, exhibits bigger aggregates than PTOBEE, with only two carbon atoms in their lateral chains. The discrete difference in their size is interpreted as due to the self-organization of both polymers in nano aggregates, by the effect of solvent.
The functionalization with choline groups increases the size of the polymers with respect to their precursor in both cases, with PTOBDME-Choline having the higher R_g values of those studied. PTOBEE-Ammonium shows even higher size aggregates than PTOBEE-Choline.
As the polymer concentration increases an evolution from rods, in the case of PTOBEE (1mg/ml) to disks and spheres (10mg/ml in all cases) is observed. (PTOBDME-Ammonium) seems to form spheres in all the studied concentrations.

The cationic ChLCP dispersed in TAE exhibit R_g values higher than those of the nucleic acids studied, and their complexes something intermediate between them, probably due to strong electrostatic interaction.

The cationic ChLCP directly get complexed with negatively charged DNA and polynucleotides in TAE suspension, presenting monodispersed globular particles with calf-thymus and plasmid DNA.

Isolated single stranded PolyA, polydT and PolyG and double stranded (PolyC-PolyG)behave as elongated rodlike particles while PolyC and PolyA-PolyT seem to be are presentas globular particles. Calf-thymus DNA, with the highest molecular weight, is probably in a supercoiled state and the DNA plasmid as globular monodispersed*collapsed coils*.

PolyA, presents a Porod slope tipical of *fully swollen coils*. In the complexes,*mass fractal networks*is formed in the case of (PTOBEE-ammonium) and (PTOBEE-choline) and *rough interface of fractal dimension* in the case of (PTOBDME-choline).

A Porod slope corresponding to *fully swollen coil* is foundfor PolydT and *rough interface of fractal dimension* for (PolydT-PTOEE-ammonium) in proportions (1:2) and (1:1). The rest of complexes seems to be as *complex mass fractal (network).*

Isolated PolyC presents a Porod slope tipical of *Gaussian chains in a dilute environment*, slightly towards a *mass fractal*. It seems to aggregate in a more globular form than the other single stranded polynucleotides. The complexes (PolyC-PTOBDME-choline) are the most voluminous with *rough interface of fractal dimension*. The rest of the polyplexes with PolyC have present *mass fractal (network)* texture.

PolyG behaves as *scattering rigid rods*. Complexes (PolyG-PTOBDME-choline) present *rough interface of fractal dimension* in the three studied proportions. Complex (PolyG-PTOBEE_ammonium) (2:1) has a slope value as *fully swollen coils*, while complex (PolyG-PTOBEE_ammonium) (1:1) approaches a *gaussian chains* structure and (PolyG-PTOBEE_ammonium) (1:2) aggregates as *mass fractal (network).* (Polyplexes PolyG-PTOBEE-choline) show*mass fractal (network)* in the three proportions.

Polynucleotide (PolyC-PolyG)dispersed in TAE, shows a gradient corresponding to fully *swollen coils* (1,6). Complexes (PolyC-PolyG-PTOBDME-choline), in the three studied proportions, present globular monodispersed aggregates with a Porod slope interpreted as due to *collapsed coils*. All proportions of complexes (PolyC-PolyG-PTOBEE-ammonium) and (PolyC-PolyG-PTOBEE-choline) exhibit globular monodispersed gradients corresponding to *mass fractals network.*

PolyA-PolyT, with the higher Porod gradient (2,8) among the polynucleotides studied, seems to be present as *globular monodispersed –collapsed coils*. The whole of their complexes show can be modelized by globular monodispersed aggregates with *collapsed coils* gradient.

The Porod gradient of isolated calf-thymus, suspended in TAE (-1,6 full) corresponds to*swollen coils.* While complexes (Calf-Thymus DNA-PTOBDME-choline) aggregate as *collapsed coils*, in all proportions, (Calf-Thymus DNA-PTOBEE-ammonium) and (Calf-Thymus DNA-PTOBEE-choline) self-associate as *mass fractal network.*

The gradient= -3,2 of the plasmid DNA, in Fig. 15, is interpreted as due to *collapsed coils* with globular particles shape. Polyplexes (Plasmid_DNA-PTOBDME-choline) and (Plasmid_DNA-PTOBEE-Ammonium (1:2) have gradients for *collapsed coils*. The rest of the complexes with Plasmid DNA have *mass fractal* Porod slopes.

The interaction between the new cationic cholesteric liquid-crystal polymers and oligonucleotides and DNA is confirmed in all the studied cases.

The new formulations are proposed as non-viral vectors for the genetic material, with potential application in Gene Therapy.

ACKNOWLEDGEMENT

The authors wish to thank the ESRF Facility for the provision of synchrotron beam at Beamline 16220.

REFERENCES

[1] a) E. Schrödinger, "*What is life? The physical aspect of the living cell"*, Cambrigdge 1945; b) E. Macías Barber, "El cristal aperiódico de la vida", RIF Noviembre 2006.
[2] a) R. E. Franklin and R.G.Goslin, Nature 171 , 740 (1953); b) M. H.F. Wilkins, A. R. Stokes and H. R Wilson , Nature 171, 738 (1953); c) J. D. Watson and F. H. C. Crick, Nature 171, 737 (1953).
[3] H. Ringsdorf, B. Schlarb, J. Venzmer, Angew. Chem. Int. Ed. Engl., 27, 113 (1988)
[4] International Union of Crystallography, Report of the Executive Committee for 1991, Acta Cryst. A48,922, (1992)
[5] a) G. Zanchetta, Liquid crystal line phases in oligonucleotide solutions, Ph.D., Thesis, University of Milan, 2007; b) A.A. Kornyshev, S. Leikin, S.V. Malinin, Chiral electrostatic interaction and cholesteric liquid crystals of DNA, Eur. Phys. J. E **7**

(2002) 83-93; c) S.L. Lai, D. Hartono, K.-L. Yang, Self-assembly of cholesterol DNA at liquid crystal/aqueous interface and its application for DNA detection, Appl. Phys. Lett. 95 (2009) 153702.

[6] a) M. Pérez-Méndez; C. Marco, "New synthesis, thermal properties and texture of cholesteric poly[ethyl ethylene 4,4'-(terephthaloyldioxy)dibenzoate]", Acta Polymerica, 48, 502-506 (1997); b) M. Pérez-Méndez.; C. Marco Rocha, " Preparing cholesteric liquid-crystals - by adding acid di:chloride and butanediol to chloro-naphthalene, heating in nitrogen, decanting into toluene, etc ", Patent with nº EP1004650-A; WO9831771-A; WO9831771-A1; AU9854863-A; ES2125818-A1; ES2125818-B1; EP1004650-A1; US6165382-A; MX9906732-A1; JP2001513827-W; AU739076-B; EP1004650-B1; DE69824182-E.

[7] J.Fayos, S.Sánchez-Cortés, C.Marco and M.Pérez-Méndez, "Conformational analysis and molecular modeling of cholesteric liquid-crystal polyesters based on XRD, Raman and transition thermal analysis", J. Macromol.Sci.-Physics, B40(3&4), 553-576 (2001).

[8] Mercedes Pérez Méndez and J. Sanguino, "Cholesteric Liquid-Crystal Copolyester, Poly[oxycarbonyl-1,4-phenylene- oxy -1,4 terephthaloyl- oxy-1,4-phenylene- carbonyloxy (1,2-dodecane)] $[C_{34}H_{36}O_8]_n$, Synthesized from Racemic Materials: Kinetics, Structure and Optical Characterization, Journal of Engineering Research and Applications , ISSN: 2248-9622, Vol. 5, Issue 7, (Part - 2) July 2015, pp.48-62

[9] M. Pérez-Méndez, J. Fayos and C.R.Mateo, "Self-assembly of cholesteric liquid-crystal polyesters and their stereoselective interaction with liposomes of DMPC ", Advances in Biochirality, Elsevier Science S. A., Chapter 24 (1999).

[10] M. Pérez-Méndez, S. Areso, A. Alarcón Vaquero, B. Elorza and M. Malfois. "Effect of polymer addition to lipid membranes as potential drug delivery systems. Structure and dynamics of their interaction", Annual Report EMBL, 372 (1998).

[11] M. Perez-Mendez, J. Fayos, G. P. Blanch and S. Sánchez Cortés, "Biofunctionalization of Cholesteric Liquid-Crystal Helical Polymers. Nanocarriers", ENCYCLOPEDIA OF NANOSCIENCE .AND NANOTECHNOLOGY 2011, Volume 11, 547-580, Edited by H. S. Nalwa, ACS. American Scientific Publishers, ISBN: 1-58883-160-4

[12] a) ATSAS2.1, P. V. Konarev, M. V. Petoukhov, V. V. Volkov and D. I. Svergun, J. of Applied Crystallography, ISSN 0021-8898, Ed: G. Kostorz; b) por D. I. Svergun, M. H. J. Koch, P. A. Timmins and R. P. May, "Small Angle X-Ray and Neutron Scattering from Solutions of Biological Macromolecules 2013, Oxford U. Press.

[13] W.F. Anderson, Human gene therapy, Nature 392 (6679 Suppl) (1998) 25-30.

[14] Ibraheem D, Elaissari A, Fessi H Gene therapy and DNA delivery systems *Int J Pharm* 2014, **459**(1-2) 70-83.

[15] M. Pérez Méndez, R. Marsal Berenguel and S: Sánchez Cortés, "New non-viral vectors based on biocompatible liquid-crystal polymers for the carriage and delivery of biomacromolecules and insoluble drugs as an strategy", Rev Oncol., 4 Suppl 1 (2002) 153.

[16] M. Pérez Méndez; R. Marsal Berenguel; S.S. Funari, "Structural Characterization of the Interaction Between Cholesteric Lquid-Crystal Polymers and Molecules of Biological Interest", HASYLAB Annual Report, 2003, 11150.

[17] M Pérez Méndez and B Hammouda, "SAXS and SANS investigation of synthetic cholesteric liquid-crystal polymers for biomedical applications", Journal of Materials Science and Engineering B 3 (2) (2013) 104-115.

[18] M Pérez Méndez, *to be published.*

[19] Boualem Hammouda, PROBING NANOSCALE STRUCTURES –THE SANS TOOLBOX. http://www.ncnr.nist.gov/staff/hammouda/the_SANS_toolbox.pdf

Figure Captions

Fig. 1. DNA crystal structure according to [2c]. Detail of double stranded PolyA-PolyT and PolyC-PolyG are shown at the right hand side.
Fig. 2. Types of Liquid-Crystal mesophases: a) Nematic, b) Smectic A and c) Cholesteric, helical pitch.
Fig. 3. Cholesteric mesophase of liquid-crystal DNA.
Fig. 4. Monomeric unit of cholesteric liquid-crystalline PTOBEE (m=1) and PTOBDME (m=9). The three different zones of the monomer: mesogen, spacer and flexible side chain are indicated. The asterisk indicates the chiral center. Torsion ϕ is indicated. Aromatic-end acid and aliphatic-end alcoholic groups are also specified.
Fig. 5. TEM images of L-α–DMPC liposomes, hexagonal when interacting with added PTOBDME.
Fig. 6. *I(q) vs* $q*R_g$curves for: (a) PTOBEE; (b) PTOBDME; (c) PTOBEE-Choline; (d) PTOBDME-Choline and (e) PTOBEE-Ammoniun.
Fig. 7. *I(q) vs q* (nm^{-1}) plots of: PolyA, PolyC, PolyG, PolydT, PolyC-PolyG, PolyA-PolydT, Calf Thymus DNA and Plasmid, in TAE.
Fig. 8. SAXS curves *I(q) vs q[*nm^{-1}*]* for PolyA in TAE and polyplexes with PTOBDME-Choline, PTOBEE-Choline and PTOBEE-Ammonium.
Fig.9. SAXS curves *I(q) vs q[*nm^{-1}*]* for PolydT in TAE and polyplexes with PTOBDME-Choline, PTOBEE-Choline and PTOBEE-Ammonium.
Fig. 10. SAXS curves *I(q) vs q[*nm^{-1}*]* for PolyC in TAE and polyplexes with PTOBDME-Choline, PTOBEE-Choline and PTOBEE-Ammonium.
Fig. 11. SAXS curves *I(q) vs q[*nm^{-1}*]* for PolyG in TAE and polyplexes with PTOBDME-Choline, PTOBEE-Choline and PTOBEE-Ammonium.
Fig. 12. (a) SAXS patterns of Complexes between PolyC-PolyG and cationic ChLCPs; (b) Fitting PolyC-PolyG to a rod model with ATSAS [12].
Fig. 13. SAXS patterns of Complexes between PolyA-PolyT and cationic ChLCPs.
Fig. 14. SAXS patterns of Complexes between Calf-Thymus DNA and cationic ChLCPs.
Fig. 15. (a) SAXS patterns of Complexes between plasmid DNA and cationic ChLCPs; (b) Fitting the plasmid to a globular monodispersed system model with GNOM (ATSAS) [12].

Tables

Table 1. Molecular weights and structure of commercial polynucleotides and nucleic acids.
Table 2. R_g values (nm) of cationic ChLCP and precursors, in TAE, calculated from the Guinier plots.
Table 3. Calculated Guinier R_g(nm) from SAXS curves, shape and fractal nature of Polyplexes with PolyA.
Table 4. Calculated Guinier R_g(nm) from SAXS curves, shape and fractal nature of Polyplexes with PolydT
Table 5. Calculated Guinier R_g(nm) from SAXS curves, shape and fractal nature of Polyplexes with PolyC
Table 6. Calculated Guinier R_g(nm) from SAXS curves, shape and fractal nature of Polyplexes with PolyG
Table 7. Calculated R_gGuinier (nm) from SAXS curves, shape and fractal nature of Polyplexes with PolyC-PolyG.
Table 8. Calculated R_gGuinier (nm) from SAXS curves, shape and fractal nature of Polyplexes with PolyA-PolyT
Table 9. Calculated R_gGuinier (nm) from SAXS curves, shape and fractal nature of Polyplexes with Calf-Thymus DNA
Table 10. Calculated R_gGuinier (nm) from SAXS curves, shape and fractal nature of Polyplexes with Plasmid_DNA